analytical chemistry

Article

Cite This: Anal. Chem. XXXX, XXX, XXX−XXX

pubs.acs.org/ac

Nanoscale Structural Organization of Plant Epicuticular Wax Probed by Atomic Force Microscope Infrared Spectroscopy

Charles Farber,[†] Rui Wang,[†] Robert Chemelewski,[†] John Mullet,[†] and Dmitry Kurouski*[,†,‡]

[†]Department of Biochemistry and Biophysics and [‡]The Institute for Quantum Science and Engineering, Texas A&M University, College Station, Texas 77843, United States

Supporting Information

ABSTRACT: The cuticle covers external surfaces of plants, protecting them from biotic and abiotic stress factors. Epicuticular wax on the outer surface of the cuticle modifies reflectance and water loss from plant surfaces and has direct and indirect effects on photosynthesis. Variation in epicuticular wax accumulation, composition, and nanoscale structural organization impacts its biological function. Atomic force microscope infrared spectroscopy (AFM-IR) was utilized to investigate the internal and external surfaces of the cuticle of *Sorghum bicolor*, an important drought-tolerant cereal, forage, and high-biomass crop. AFM-IR revealed striking heterogeneity in chemical composition within and between the surfaces of the cuticle. The wax aggregate crystallinity and distribution of chemical functional groups across the surfaces was also probed and compared. These results, along with the noninvasive nondestructive nature of the method, suggest that AFM-IR can be used to investigate mechanisms of wax deposition and transport of charged molecules through the plant cuticle.

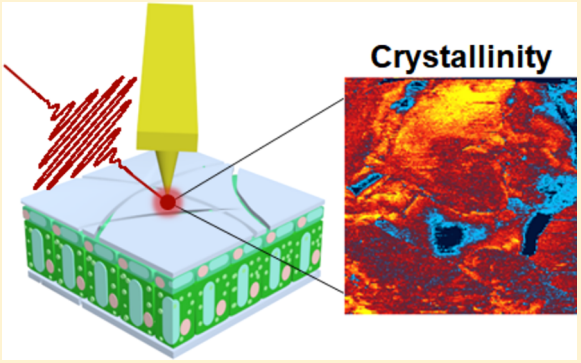

INTRODUCTION

The cuticle plays a vital role in plant protection against agricultural pests and abiotic stresses such as drought and heat and affects canopy reflectance, photosynthesis, and water use efficiency.[1−3] Epicuticular waxes enriched in the outer layer of the cuticle are primarily composed of long-chain chemically modified hydrocarbons that are secreted by epidermal cells.[4] The composition and structure of waxes and other chemicals that accumulate on the surfaces of plants varies by organ, cell type, developmental stage, and environmental conditions. Sorghum (*Sorghum bicolor*) accumulates significant levels of wax on its leaf, leaf sheath, and stem surfaces to minimize water loss during drought conditions, lending to its worldwide distribution.[1,2] Sorghum epicuticular wax is enriched long-chain hydrocarbons that are valuable bioproducts.[5,6]

Chemical characterization of plant waxes is typically conducted following extraction with solvents such as hexane, diethyl ether, and chloroform, followed by HPLC analysis.[7] Extracted sorghum and maize waxes were separated by the Bianchi group on a silica gel column using carbon tetrachloride to elute alkanes, esters, and aldehydes, chloroform to elute alcohols, and chloroform/acetic acid to elute acids.[8,9] Results are typically reported in percentages of compounds present from each chemical class. Accurate and quantitative wax analysis by HPLC has been a challenging task because most wax components have no UV chromophore and cannot be detected using standard UV−vis detection modules. Wax is also poorly soluble at room temperature, so it must be melted and dissolved before applying it to the column or during HPLC analysis, treatments that could change its composition. Separation and quantitation of wax components with currently available columns is challenging.[7] However, recent developments in HPLC, such as coupling with evaporative light-scattering detection, have resulted in higher sensitivity and quantitative power.[10] Ultimately, results of HPLC analysis of plant waxes are sometimes inconsistent.[11,12]

Some of these limitations can be overcome by using mass spectrometry (MS) coupled to HPLC or by time-of-flight secondary ion mass spectrometry (TOF-SIMS). Recently, Kulkarni and co-workers reported analysis of *Populus trichocarpa* leaf surfaces using TOF-SIMS.[13] The researchers identified that long-chain aliphatic saturated alcohols (C_{21}−C_{30}), hydrocarbons (C_{25}−C_{33}), and wax esters (WEs; C_{44}−C_{48}) were present in the wax layers of leaf surfaces. Coupling this technique to principal component analysis (PCA), Kulkarni et al. characterized the distribution of these molecules with 1 μm spatial resolution. The Popp group suggested the use of coherent anti-Stokes Raman scattering (CARS) for imaging epicuticular waxes on the surface of plants.[14] Unlike MS, CARS is noninvasive and nondestructive, allowing for in vivo imaging of plants. In their proof-of-principle study, Weissflog and co-workers imaged the distribution of hydrocarbons by analysis of CH_2-stretching vibrations of the epicuticular wax at 2845 and 2880 cm^{-1}. Similar results were

Received: November 15, 2018
Accepted: January 9, 2019
Published: January 9, 2019

DOI: 10.1021/acs.analchem.8b05294
Anal. Chem. XXXX, XXX, XXX−XXX

achieved by Greene and Bain upon spectroscopic analysis of barley leaf surfaces using total internal reflection Raman spectroscopy (TIR-RS).[15] It would be valuable to determine the distribution of other chemical components of epicuticular waxes, such as esters or aldehydes. Additionally, both TIR-RS and CARS are diffraction-limited techniques, limiting their spatial resolution down to approximately one-half of the wavelength of light used for sample imaging.

Scanning probe microscopy (SPM) techniques, such as atomic force microscopy (AFM), are not hindered by the diffraction limit, unlike light-based techniques.[16] Additionally, SPM can be noninvasive and nondestructive. Using this advantage of AFM, Koch and co-workers imaged wax regeneration on the surface of *Galanthus nivalis* leaves.[17] The researchers observed the growth of individual wax layers with 3−5 nm thickness. AFM provides surface topography data, rather than chemical information. The coupling of AFM to vibrational spectroscopy, such as Raman or infrared, would be advantageous for simultaneous acquisition of chemical and topographical information about samples with subdiffraction limit spatial resolution.[18−21]

AFM-IR is a spectroscopic technique that combines AFM and Infrared spectroscopy.[22−24] In AFM-IR, a sample is irradiated by pulsed infrared (IR) radiation with an AFM tip in proximity to its surface. As the laser sweeps through its tuning range, the sample expands based on how well its components absorb at different wavelengths. Sample expansion causes the tip to oscillate; these oscillations, following Fourier transformation, directly correspond to the IR spectrum of the sample. Consequently, AFM-IR is capable of providing chemical information about the sample surface with subdiffraction limit spatial resolution.[25] The probe is placed on top of the surface being analyzed and can be withdrawn from the sample's surface after spectral acquisition, which makes this analytic technique noninvasive and nondestructive. AFM-IR has been utilized to investigate various topics in biology and surface chemistry including malaria-infected blood cells,[26] $CH_3NH_3PbI_3$ polycrystalline perovskite films,[27] and bacteria.[28]

In this study, we utilized AFM-IR to characterize the nanoscale structural organization of internal and external surfaces of epicuticular wax that covers the stems of sorghum plants. Our results demonstrate that AFM-IR allows nanoscale analysis of epicuticular wax heterogeneity. Using AFM-IR, we were able to identify wax clusters with different intensity of CH_2 vibrations, suggesting different degrees of crystallinity. Moreover, we were able to characterize the distribution of carbonyls on internal and external surfaces of the wax layer and better understand the topography of this biological polymer. These results indicate that this noninvasive and nondestructive spectroscopic technique can be used for in vivo studies of wax deposition and analysis of changes in wax structure and composition in response to biotic and abiotic stresses.

METHODS

Sorghum Plants. Sorghum (*Sorghum bicolor* strain BTx398) plants were individually grown in 3.8 gallon pots using a potting soil mix (SunGro Professional Mix #1, Bellevue, WA) in a greenhouse in College Station, TX, and harvested after 87 days. Plants were maintained under well-watered conditions and fertilized with Osmocote (Scotts Co., Marysville, OH) slow-release formulation. Plants were harvested 12 h after last watering and moved into a 4 °C environment for processing. Processed plant parts were stored at 4 °C after processing, prior to wax extraction.

Sorghum Wax Extraction and Preparation. All wax studied was taken from the middle internode of the plant. A razor blade was used to peel up a section of the stem tissue, cracking the wax attached to the surface. The wax was then removed from the surface using tweezers and directly used for ATR-IR. Due to the invasive nature of this extraction, it is impossible to determine whether only the epicuticular waxes or the whole plant cuticle was removed. Therefore, it is possible that small fractions of cuticle membrane could be present on the internal surface of epicuticular wax. Wax samples for AFM-IR or SEM were adhered stem-side in or stem-side out to 12 mm AFM discs (Ted Pella, Inc. Redding, CA) using double-sided scotch tape and stored at 4 °C prior to data collection.

AFM-IR. AFM-IR analysis was conducted using a Nano-IR2-s system (Anasys Instruments Inc., Santa Barbara, CA). The IR source was an optical parametric oscillator (OPO) laser, with a 1 kHz pulse rate and a 10 ns pulse length. Contact mode AFM tips (Anasys Instruments Inc., Santa Barbara, CA) with a resonance frequency of 13 ± 4 kHz and a spring constant of 0.007−0.4 N/m were used to obtain all spectra and maps. The system was purged with N_2 to control humidity. Single spectra were obtained in the ranges of 900−2100 and 2500−3600 cm^{-1} with a resolution of 4 cm^{-1}, and IR maps at different wavenumber values were obtained to study the distribution of wax components. AFM height and deflection images were acquired simultaneously with the IR maps. To determine whether the laser or tip would damage the surface, repeated scans of the same region of external wax were acquired and compared (Figure S1). This analysis revealed no evidence of laser or tip-induced damage to the surface. Spectra were smoothed with the Analysis Studio's (Anasys Instruments Inc., Santa Barbara, CA) built-in smoothing function using 2 points. Smoothed spectra were then imported into the MATLAB R2017b (Mathworks, Natick, MA) addon PLS_toolbox 8.6.1 (Eigenvector Research Inc., Manson, WI) for spectral averaging. AFM and IR map images were processed using built-in Analysis Studio functions.

ATR-FTIR. Attenuated total reflection (ATR)-FTIR readings were taken using a Thermo Nicolet 380 Spectrometer (Thermo Fisher Scientific, Waltham, MA) with a Smart Orbit ATR attachment using a diamond crystal. Spectra were recorded with a resolution of 4 cm^{-1} in the range of 4000−400 cm^{-1}. A background spectrum was acquired immediately before the measurement. Wax was extracted as previously described and deposited onto the crystal. The wax was not intact for these readings. The spectrum was recorded and ATR corrected using OMNIC software (Thermo Fisher Scientific).

Surface Characterization by Scanning Electron Microscopy (SEM). Scanning electron microscopy (SEM) images were taken using a JEOL JSM-7500F ultrahigh-resolution field emission scanning electron microscope with an operating voltage of 10 kV. Prior to SEM imaging, samples were coated with 5 nm of Au using a Cressington Sputter Coater (Watford, United Kingdom).

RESULTS AND DISCUSSION

Scanning Electron Microscopy (SEM) Characterization of Stem Wax. The external wax surface (EX-WS) has a flat uniform topography comprised of tightly packed brick-like aggregates, as evident from the SEM images shown in Figure 1. The internal wax surface (IN-WS) exhibits smooth topography

DOI: 10.1021/acs.analchem.8b05294
Anal. Chem. XXXX, XXX, XXX−XXX

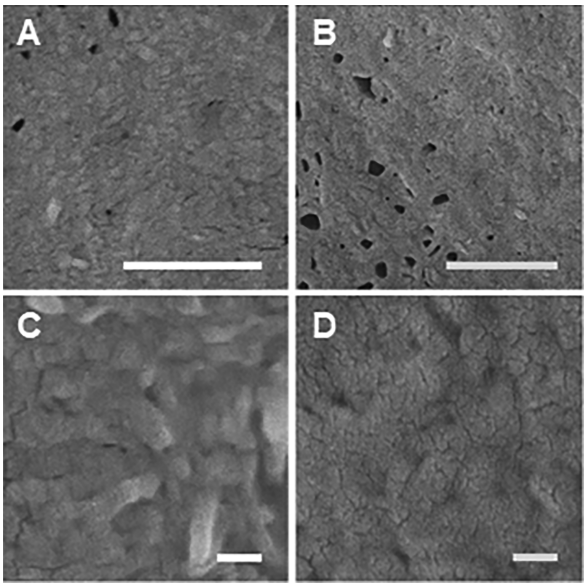

Figure 1. SEM images of the external (A and C) and internal (B and D) surfaces of sorghum stem wax. Scale bars: 1 μm (A and B) and 100 nm (C and D).

without any distinct features. We observed cracks and perforations of varying shapes and sizes on both sides of epicuticular wax layers.

Spectral Characterization of Stem Wax. AFM-IR spectra from both EX-WS and IN-WS exhibited vibrational bands around 980−1004 cm^{-1} (Figure 2) that could be assigned to C−O stretching vibrations (Table 1). This indicates the presence of carbohydrates on both surfaces of sorghum stem wax. Interestingly, the intensity of these bands varied in spectra collected at different locations on EX-WS and IN-WS. This indicates that the distribution of carbohydrates is not uniform across the wax surface.

In the AFM-IR spectra collected from EX-WS, we observed vibrational bands in 1108−1172 cm^{-1} spectral region, which could be assigned to C−O vibrations of secondary saturated, secondary unsaturated, and/or tertiary alcohols. Interestingly, on EX-WS, we did not observe vibrational bands in the 1030−1080 cm^{-1} spectral region that correspond to primary or unsaturated alcohols; however, these vibrational bands were observed on IN-WS (discussed below). Bands in this region could also be assigned to the vibrations of sugars, which is reasonable as the cuticle (which would be attached to the IN-WS) contains sugars.

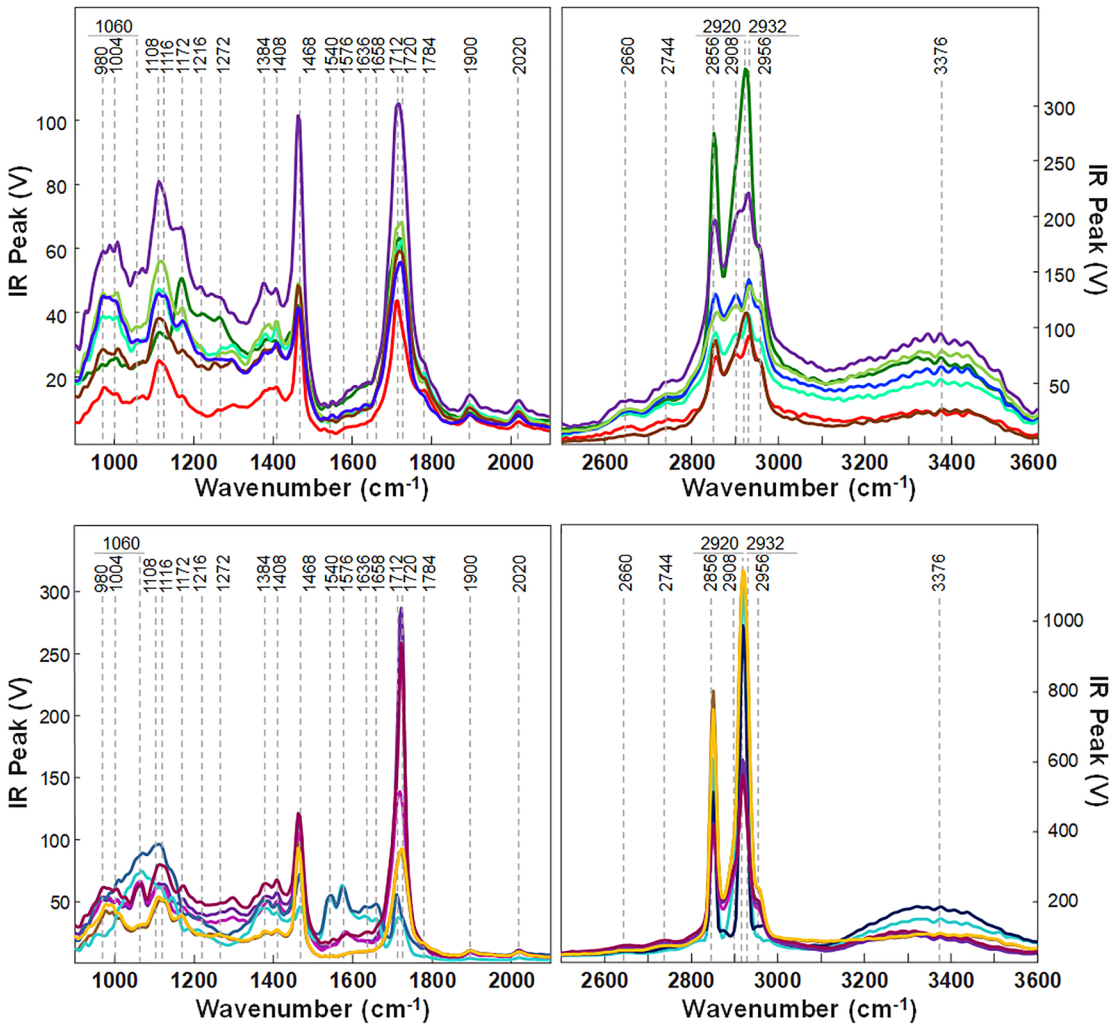

Figure 2. AFM-IR spectra collected from EX-WS (top panel) and IN-WS (bottom panel) of sorghum. Class 1 is indicated by the yellow and dark yellow spectra; Class 2 is indicated by purple, maroon, fuchsia; Class 3 is indicated by light and dark blue.

DOI: 10.1021/acs.analchem.8b05294
Anal. Chem. XXXX, XXX, XXX−XXX

Table 1. Vibrational Bands and Their Assignments for Sorghum Stem Wax

band [cm^{-1}]	vibrational mode	assignment[29,30]
980−1004	C−O stretching	carbohydrates
1030−1080	C−O stretching	R−CH_2−OH (1° alcohols) and C═C−CH_2−OH (1° unsaturated alcohols), C−O−C glycosidic vibrations, or C−O vibration of carbohydrates
1108−1172	C−O stretching	RR′CH−OH (2° alcohols), C═C−CRR′−OH (2° unsaturated alcohols), and RR′R′′−OH (3° alcohols), C−O−C glycosidic vibrations, or C−O vibration of carbohydrates
1216	symmetric ═C−O−C stretching	Ar−O−R (aromatic ethers)
1272	asymmetric ═C−O−C stretching	Ar−O−R (aromatic ethers)
1384−1408	C−H bending	alkanes
1468	CH_2 scissoring	alkanes
1540−1576	ring C═C stretching	aromatic ring
1636−1658	C═O stretching	R−C(O)−NH−R′ (proteins)
1712−1720	C═O stretching	RR′C═O (ketones), R−CH═O (aldehydes), C═C−C(O)−O−R (unsaturated esters), and R−C(O)−OH (carboxylic acids)
1715−1730	C═O stretching	Ar−C(O)−O−R (aromatic esters)
1760−1790	C═O stretching	R−C(O)−O−Ar (aromatic esters)
1900	aromatic overtones	aromatics
2020	aromatic overtones	aromatics
2660−2744	C−H stretching	R−CH═O (aldehydes)
2856	symmetric CH_2 stretching	alkanes
2908−2932	asymmetric CH_2 stretching	alkanes
2956	C−H stretching	alkanes
3300−3400	O−H stretching	alcohols

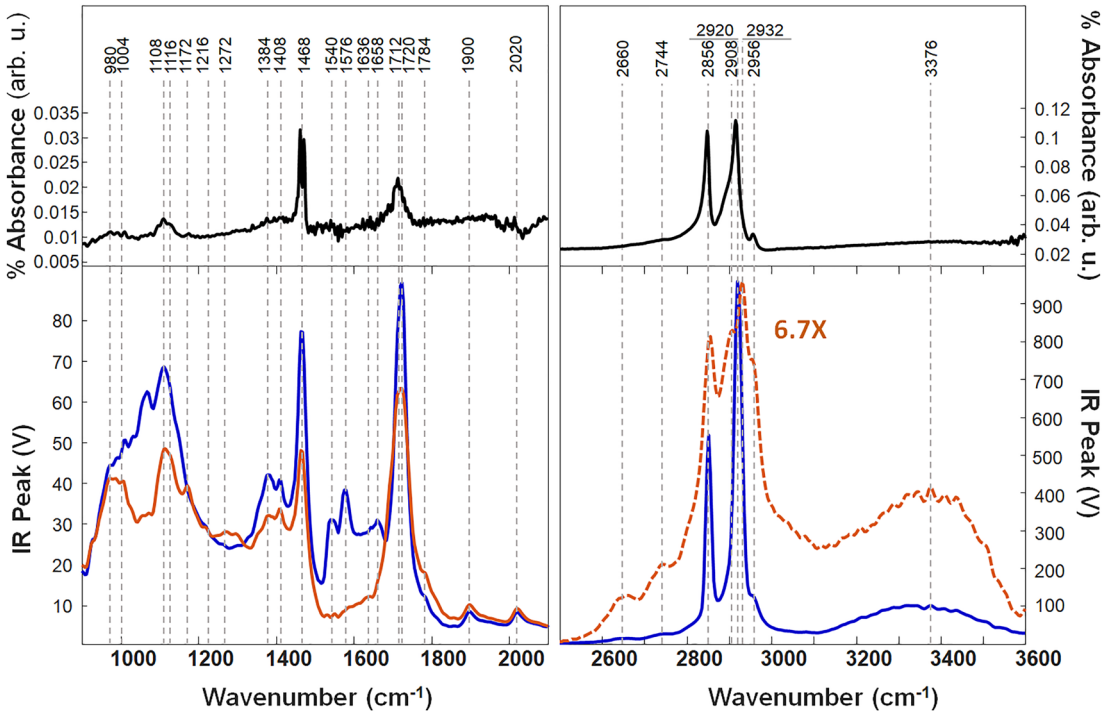

Figure 3. ATR-FTIR spectrum of sorghum wax (black) and averaged AFM-IR spectra collected from EX-WS (orange) and IN-WS (blue) of sorghum.

On the basis of this observation, we conclude that various alcohols are present in epicuticular wax of sorghum where IN-WS has a more diverse composition of alcohols compared to EX-WS. As previously seen in the unsaturated hydrocarbons, C−O vibrational intensities varied both within and between the EX- and IN-WS. This suggests there is an uneven distribution of alcohols on both EX-WS and IN-WS of sorghum stems. For instance, in most of the spectra collected from EX-WS, bands at 1108−1116 cm^{-1} are more intense compared to the 1172 cm^{-1} band, suggesting that secondary and/or secondary unsaturated alcohols predominate in EX-WS.

However, in some spectra (Figure 2 (top panel, green)), the vibrational band at 1172 cm^{-1} is more intense than the 1108−

DOI: 10.1021/acs.analchem.8b05294
Anal. Chem. XXXX, XXX, XXX−XXX

1116 cm^{-1} bands, indicating predominance of tertiary alcohols at this surface location. We also observed a broad vibrational band at 3300−3400 cm^{-1} in AFM-IR spectra collected from both EX-WS and IN-WS, confirming the presence of alcohols on their surfaces. The intensity of this band varies across the EX-WS and IN-WS surfaces, indicating an uneven distribution of alcohols in the epicuticular wax layer. It is also possible that the differences in intensity of this band are associated with differences in sample stiffness between the top and the bottom layers of the wax. Interestingly, this band is nearly twice as intense in the averaged spectrum of IN-WS than in the averaged AFM-IR spectrum of the EX-WS (Figure 3). This indicates that the concentration of alcohols on IN-WS is nearly double that of EX-WS. Additionally, we observed two vibrational bands at 1216 and 1272 cm^{-1} in some spectra collected from EX-WS (purple and green).

These vibrations correspond to =C−O−C symmetric and asymmetric stretches of aromatic ethers (Ar−O−R). These bands were not detected in the AFM-IR spectra collected from IN-WS. This observation indicates that EX-WS of sorghum stems contains aromatic ethers that are not evident on IN-WS.

AFM-IR spectra collected from both EX-WS and IN-WS contained vibrational bands at 1384−1408 cm^{-1}, which correspond to C−H bending of CH_3 groups. Additionally, we observed intense bands at ∼1468 cm^{-1} that correspond to CH_2 scissoring vibration of alkanes. This class of chemical compounds also exhibits vibrations in the 2850−2950 cm^{-1} spectral region. Specifically, a band at 2856 cm^{-1} corresponds to symmetric CH_2 stretching and a band at 2930 cm^{-1} to asymmetric CH_2 stretching, whereas vibrational bands around 2956 cm^{-1} correspond to the antisymmetric C−H stretching of CH_3 groups. The maxima of CH_2 stretching bands varied from 2908 to 2932 cm^{-1} in the AFM-IR spectra from EX-WS. This is typical for different conformations that can be adopted by aliphatic chains and suggests that AFM-IR can probe local conformations of aliphatic chains in plant epicuticular waxes. In addition, in the AFM-IR spectra collected from IN-WS, only 2932 cm^{-1} bands corresponding to asymmetric CH_2 stretching are visible and the 2856 and 2932 cm^{-1} bands are nearly seven times as intense in AFM-IR spectra of IN-WS compared to EX-WS (Figure 3). Such intense 2856 and 2932 cm^{-1} bands with an absence of bands at 2908 and 2920 cm^{-1} are typical for a crystalline wax.[31] Therefore, we conclude that wax on IN-WS has a more highly ordered structure compared to the EX-WS; alternatively, the IN-WS may have a higher abundance of long-chain CH_2 groups than the EX-WS. It is possible that EX-WS is exposed to mechanical stress and other environmental factors that disrupts organization of aliphatic chains of epicuticular waxes.

AFM-IR spectra from both EX-WS and IN-WS exhibited strong bands in a carbonyl region (1700−1750 cm^{-1}) of electromagnetic spectrum. We found that this band has two maxima at 1712 and 1720 cm^{-1} in all AFM-IR spectra. These vibrations were tentatively assigned to ketones, aldehydes, unsaturated (C=C−C(O)−O−R) or aromatic (Ar−C(O)-O-R) esters, and carboxylic acids. However, carboxylic acids typically exhibit a broad band around 2600−2990 cm^{-1} (O−H stretch), which is not observed in the AFM-IR spectra. This band is characteristic of short-chain carboxylic acids; however, longer chain acids, such as those that may be in this wax, do not display this O−H band but rather only the carbonyl band (∼1720 cm^{-1}), whose position is shared with other carbonyl-containing compounds. Thus, we cannot conclude whether carboxylic acids were present in our sample from our analysis. Aliphatic esters (R−C(O)−O−R) typically exhibit carbonyl vibration at 1735−1750 cm^{-1}, which is also observed in the AFM-IR spectra. On the basis of this spectral analysis we conclude that EX-WS and IN-WS contain ketones, aldehydes, unsaturated (C=C−C(O)−O−R), or aromatic (Ar−C(O)-O−R, 1715−1730 cm^{-1} and R−C(O)−O--Ar, 1760−1790 cm^{-1}) esters. More accurate assignment of observed carbonyl vibrations requires mass spectroscopic analysis of sorghum wax that is beyond the scope of the current work.

The intensity of carbonyl bands varies at different locations in EX-WS and IN-WS. This suggests an uneven distribution of carbonyl-containing compounds on the wax surface. Also, the intensity of carbonyl bands in some of AFM-IR spectra of IN-WS is much higher than EX-WS (Figure 3). This indicates a higher concentration of carbonyl-containing compounds on IN-WS compared to EX-WS derived from sorghum stems. Moreover, the high intensity of the carbonyl bands often correlates with the presence of 1540−1576 cm^{-1} bands (aromatic ring vibrations) in these spectra. This strongly suggests the presence of aromatic esters in this surface.

Vibrational bands around 2660 and 2744 cm^{-1} can be assigned to C−H stretching of aldehydes. This indicates that aldehydes are present on both EX-WS and IN-WS of sorghum, a topic of previous debate.[8,11,12] The intensity of these bands varied across the IN-WS and EX-WS surfaces. This indicates that the distribution of aldehydes is not uniform across the wax surfaces.

AFM-IR spectra that can be assigned to the second class (purple spectra in Figure 2, bottom) have higher variations in intensities of all vibrational bands that were observed for the first class of spectra. We also observed an intense band at 1060 cm^{-1} in this group of spectra that can be assigned to C−O stretching of primary and unsaturated alcohols that were not evident in EX-WS nor in the first class IN-WS spectra. The third class (blue spectra in Figure 2, bottom) of AFM-IR spectra has intense vibrational bands centered at 1540 and 1576 cm^{-1} that can be assigned to aromatic ring vibrations, indicating the presence of aromatic compounds on IN-WS. These vibrational bands were not observed in the AFM-IR spectra collected from EX-WS. We also observed two vibrational bands at 1636 and 1658 cm^{-1} in some spectra acquired on IN-WS. These bands could be assigned to amide vibrations of proteins that have unordered and α-helical secondary structure, indicating the presence of proteins on the IN-WS. Additionally, these spectra exhibit a broad band spanning from ∼1000 to 1200 cm^{-1} in place of the well-defined peaks seen in the other two classes.

A question to address in future studies is why the concentration of alcohols, carbonyl-containing and aromatic compounds, and proteins is higher on IN-WS vs EX-WS. These compounds are likely to perform physiological functions at wax−-cellular interfaces by being a part of a "spacing" layer between cell walls and IN-WS. Alternatively, differences in the concentrations of these compounds could be due to lower stability on the external surface compared to the internal. Finally, observed differences could be due to changes in the composition of secreted epicuticular wax during plant development or plant growth.[32] This hypothesis is currently being tested by spectroscopic examination of waxes of young and older internodes of sorghum.

Attenuated total reflection (ATR)-FTIR is a classical tool for determination of a chemical structure of plant waxes (Figure

DOI: 10.1021/acs.analchem.8b05294
Anal. Chem. XXXX, XXX, XXX−XXX

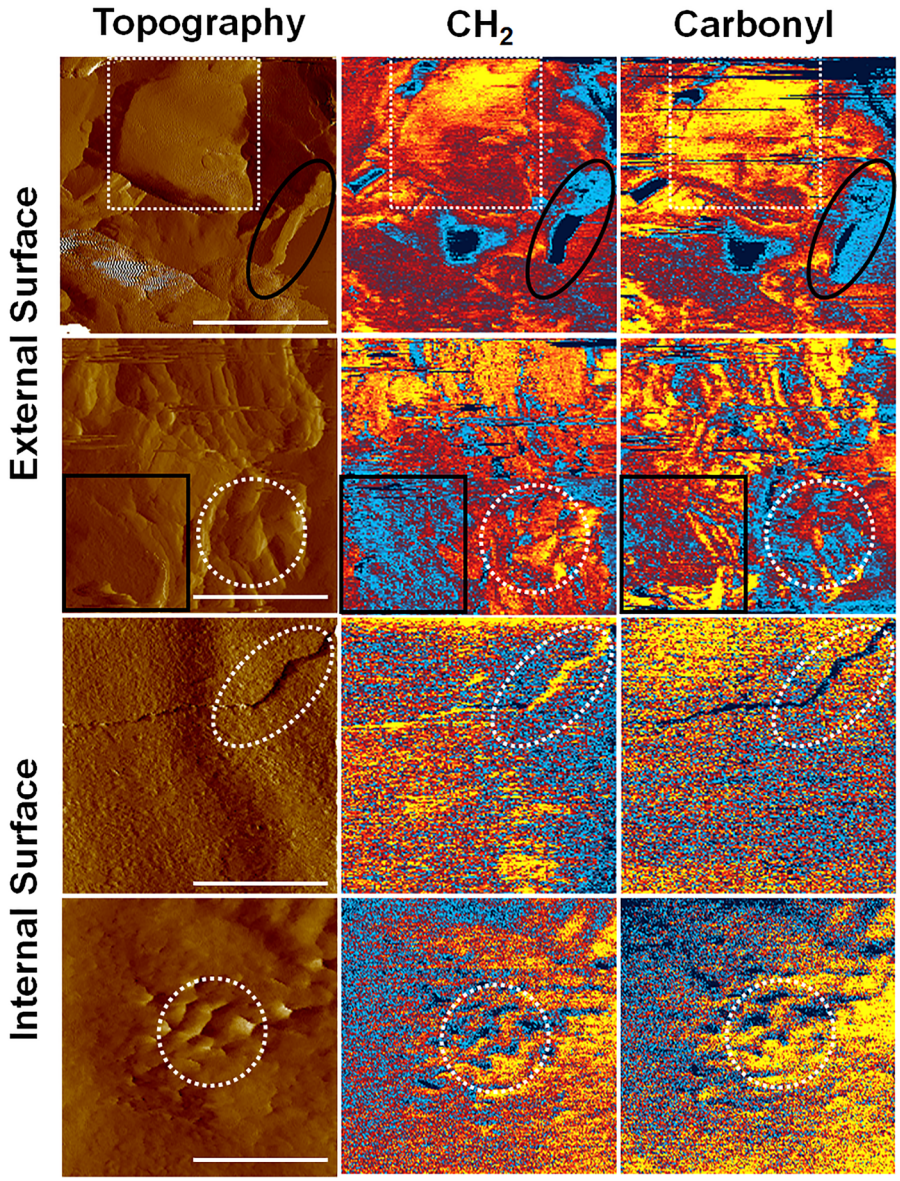

Figure 4. Nanoscale structural organizations of EX-WS and IN-WS of *Sorghum bicolor* probed by AFM-IR. EX-WS (two top rows) and IN-WS (bottom two rows) have different topography. IN-WS has smooth topography, whereas EX-WS contains a variety of aggregates with different shapes and sizes. Nano-IR reveals different intensities of CH_2 and carbonyl groups on the surface of these wax clusters. For the external surface, white dashed shapes indicate regions of higher intensity and black solid shapes lower intensity. For the internal surface, white dashed shapes indicate interesting features. Maps were acquired at 1450 cm^{-1} for CH_2 and 1725 cm^{-1} for carbonyl. To improve image clarity, raw IR images were flattened using the Analysis Studio software; then the modulus of the resulting height was taken to make all values positive or zero. Heights for the maps are as follows. For EX: (top left) 0.1 V; (top right) 0.16 V; (bottom left) 0.11 V; (bottom right) 0.35 V. For IN: (top left) 0.09 V; (top right) 0.09 V; (bottom left) 0.06 V; (bottom right) 0.20 V. Yellow indicates closer to the max height and blue further from the max height. Scale bars: 5 μm.

3).[30,33] ATR-FTIR can be used to detect the presence of unsaturated hydrocarbons (980−1004 cm^{-1}) as well as alcohols. However, only the presence of secondary and secondary unsaturated alcohols can be identified from the ATR-FTIR spectrum of wax, whereas no information about primary and tertiary alcohols is obtained. Also, evidence of CH vibrations of CH_3 groups of hydrocarbons could not be obtained via ATR-IR analysis of wax, whereas these vibrations were clearly identified in the AFM-IR spectra of sorghum wax. We observed a doublet of peaks around 1468 cm^{-1} in the ATR-FTIR spectrum of wax, whereas these two peaks could not be fully resolved in AFM-IR spectra of IN-WS and EX-WS. Finally, we observed a carbonyl band centered around 1710 cm^{-1} in the ATR-FTIR spectrum of sorghum wax. Interestingly, neither peak at 1784 cm^{-1} (R−C(O)−O−Ar) could be identified in the ATR-FTIR of sorghum wax nor aromatic vibrations (1540−1576 cm^{-1}). This suggests that the low amounts of these chemical compounds in epicuticular wax can only be identified using AFM-IR.

Analysis of the 2600−3600 cm^{-1} region of the ATR-FTIR spectrum indicates that only symmetric and asymmetric CH_2 stretching (2856−2930 cm^{-1}) as well as C−H stretching of alkanes (2956 cm^{-1}) can be observed. The spectral pattern of these bands is very similar to AFM-IR spectra of IN-WS. Thus, one may conclude that ATR-FTIR is not capable of probing deformations of alkane chains that are typical for EX-WS. It is

DOI: 10.1021/acs.analchem.8b05294
Anal. Chem. XXXX, XXX, XXX−XXX

also possible that these signals are lost due to the larger sample volume probed by ATR compared to AFM-IR. At the same time, ATR-IR spectra suggest that the bulk volume of sorghum stem wax has an ordered or highly crystalline wax structure, which was only observed at IN-WS by AFM-IR.

AFM-IR Imaging of EX- and IN-WS. AFM-IR imaging revealed the nanoscale structural organization of sorghum epicuticular wax. We found that EX-WS has an uneven distribution of alkane chains and carbohydrates (CH_2 and C−O), alcohols (R−OH and −OH), as well as and carboxyl groups (C═O) across the wax surface (Figure 4 and Figures S2 and S3). Carbonyls typically exhibit high intensity at the edges of wax aggregates, whereas flat terraces of these wax clusters may or may not show intense carbonyl vibrations. It has been also found that areas with weak CH_2 vibrations exhibit strong R−OH and OH signals, indicating the presence of alcohols on those surface sites.

We also found that chemical images allow for visualization of shapes of various aggregates on the wax surface. As described above, EX-WS contains a variety of wax clusters of different shapes and sizes. We found that some of them (Figure 4, white dashed square and circle) exhibit high intensity (0.1 V, top center), whereas others have a lower intensity of CH_2 vibrations (0.002 V, top center, black oval). This suggests different degrees of aliphatic chains' order in these wax clusters, which can also be considered in terms of wax crystallinity.[34,35] Historically, crystallinity of substances such as wax has been assessed using polarized light microscopy.[36] As this method is based on inspection of crystals by eye, it is resolution limited. In terms of X/Y, crystals can be resolved down to approximately 0.5 um due to the diffraction limit. Our method is a nondiffraction-limited way to study the nanoscale crystallinity. We also observed small changes in CH_2 vibrations even within the single wax clusters (Figure 4, white dashed square). This observation suggests that AFM-IR can be used to visualize nanoscale structural organization of individual wax aggregates that were not revealed by AFM or SEM. We also found that the intensity of carboxyl bands does not directly correlate with high and low intrinsic order of wax aggregates. In some areas with low intensity of CH_2 vibrations, carbonyls were more intense, whereas in other areas with low intensity of CH_2 vibrations, the intensity of carbonyls is correspondingly low.

AFM-IR imaging ofan internal wax surface confirmed its flat, smooth morphology, previously observed with SEM. We observed two major classes of nanofeatures on its surface: wax edges and pores. We found that wax at edges has a high intensity of CH_2 vibrations and low intensity of carbonyls compared to the wax on plateaus around these areas. As was discussed above, newly formed wax has higher intensity of CH_2 vibrations comparing to the old or aged wax. This observation suggests that wax growth may occur at wax edges by a templating mechanism, where a previously formed edge of wax serves as a template for arrangement of newly secreted aliphatic chains. Interestingly, these newly forming areas of wax have a low intensity of carbonyls. We also found that the edges of pores on the internal surface of wax have a high intensity of both CH_2 and carbonyl vibrations. These pores could be involved in secretion of constituents of wax layers that were synthesized by plant cells into the outer layers of wax.

The presence of such pores was previously predicted by a series of elegant experiments performed by the Schönherr group.[37−39] Using simulation of foliar uptake (SOFU), the researchers demonstrated that charged molecules can diffuse across isolated cuticles. Since such charged analytes carry hydration shells, they cannot be soluble in lipophilic wax domains of waxes. Therefore, it has been proposed that charged molecules travel through aqueous polar pores present in the wax layer. These experiments also demonstrated that cuticle and epicuticular wax layers are dynamic rather than static systems.[40] Consequently, noninvasive and nondestructive AFM-IR is ideally suited for monitoring such structural changes that are taking place in the cuticle and epicuticular wax layers during plant growth and development as well as following plant exposure to biotic and abiotic stresses.

We also expect that AFM-IR will shed light on mechanisms of fungal, bacterial, and viral infections of plants.[41] It has been shown that after landing on a plant surface, fungal spores of some species, for example, *Erysiphe graminis*, release a liquid that erodes the leaf surface, making it more hydrophilic.[42] This helps the spores to affix onto the plant surface. Several hours after spore adhesion, a germ tube of the spore penetrates the plant surface, infecting the host. Using AFM-IR, the chemical nature of spore-induced modifications of plant surfaces can be revealed. This information can be used to guide the synthesis of pesticides toward more efficient and minimally toxic chemicals that would have high retention on plant surfaces. Additionally, chemical imaging of plant waxes, which was demonstrated in the current study, can be used to develop models that will predict the duration of retention of pesticides and other xenobiotic compounds on plants.[43] This is highly important to increase their economic efficiency and prevent consumption of these chemicals by humans.

CONCLUSIONS

The potential of AFM-IR as a method for the noninvasive nondestructive characterization of epicuticular plant waxes was demonstrated. Point spectra acquired from IN-WS and EX-WS of sorghum stems revealed heterogeneity of chemical composition both within and between these two surfaces. We showed how the intensities of the CH_2 stretching bands vary between the inner and the outer surfaces of epicuticular wax. Our results indicate that the outer surface of wax has disordered aliphatic hydrocarbons, whereas the inner side of epicuticular wax assumes a more ordered, crystalline conformation. We also found that while the ATR-FTIR and AFM-IR spectra agree well, there are some chemical features only captured by AFM-IR, such as the disorganization of aliphatic chains on the outer wax layer, indicating that AFM-IR may have higher site specificity than ATR-FTIR. Finally, using chemical mapping, we cross-correlated the distributions of carbonyl and CH_2 groups to the surface topography and each other. We observed wax edges with high CH_2 intensity, suggesting wax growth via a templating mechanism. Together, these results indicate that AFM-IR is a favorable technique for in vivo studies of plant wax secretion during development and under different stress conditions.

ASSOCIATED CONTENT

Supporting Information

The Supporting Information is available free of charge on the ACS Publications website at DOI: 10.1021/acs.analchem.8b05294.

AFM-IR data collection parameters; AFM topography and chemical maps of the same wax region scanned

DOI: 10.1021/acs.analchem.8b05294
Anal. Chem. XXXX, XXX, XXX−XXX

sequentially at 1450, 1725, and 1900 cm^{-1}; AFM (topography) and chemical images of carbohydrate (984 cm^{-1}), alcohol R−OH (1120 cm^{-1}), carbonyl (1725 cm^{-1}), aliphatic (1450 cm^{-1}), and alcohol O−H (3400 cm^{-1}) bands of EX-WS; deflection images corresponding to the chemical maps in Figure S2 (PDF)

AUTHOR INFORMATION

Corresponding Author

*E-mail: dkurouski@tamu.edu. Tel: 979-458-3778.

ORCID

Dmitry Kurouski: 0000-0002-6040-4213

Notes

The authors declare no competing financial interest.

ACKNOWLEDGMENTS

We are grateful to AgriLife Research of Texas A&M for the provided financial support. We also acknowledge the Governor's University Research Initiative (GURI) grant program of Texas A&M University, GURI Grant Agreement No. 12-2016. Use of the TAMU Materials Characterization Facility and Dr. Yordanos Bisrat are acknowledged.

REFERENCES

(1) Jordan, W. R.; Shouse, P. J.; Blum, A.; Miller, F. R.; Monk, R. L. *Crop Sci.* **1984**, *24*, 1168−1173.
(2) Burow, G.; Franks, C. D.; Xin, Z. *Crop Sci.* **2008**, *48*, 41−48.
(3) Awika, H. O.; Hays, D. B.; Mullet, J. E.; Rooney, W. L.; Weers, B. D. *Euphytica* **2017**, *213*, 207.
(4) Bernard, A.; Joubes, J. *Prog. Lipid Res.* **2013**, *52*, 110−129.
(5) Jenks, M. A.; Rich, P. J.; Rhodes, D.; Ashworth, E. N.; Axtell, J. D.; Ding, C. K. *Phytochemistry* **2000**, *54*, 577−584.
(6) Hwang, K. T.; Cuppett, S. L.; Weller, C. L.; Hanna, M. A. *J. Am. Oil Chem. Soc.* **2002**, *79*, 521−527.
(7) Jetter, R.; Kunst, L.; Samuels, A. L. In *Annual Plant Reviews, Biology of the plant cuticle*, Riederer, M.; Müller, C., Eds.; Blackwell Publishing: Oxford, United Kingdom, 2008, pp 145−181.
(8) Avato, P.; Bianchi, G.; Murelli, C. *Phytochemistry* **1990**, *29*, 1073−1078.
(9) Bianchi, G.; Avato, P.; Mariani, G. *Cereal Chem.* **1979**, *56*, 491−492.
(10) Nayak, V. S.; Tan, Z.; Ihnat, P. M.; Russell, R. J.; Grace, M. J. *J. Chromatogr. Sci.* **2012**, *50*, 21−25.
(11) Bianchi, G.; Avato, P.; Salamini, F. *Maydica* **1975**, *20*, 165−173.
(12) Dalton, J. L.; Mitchell, H. L. *J. Agric. Food Chem.* **1959**, *7*, 570−573.
(13) Kulkarni, P.; Dost, M.; Bulut, Ö. D.; Welle, A.; Böcker, S.; Boland, W.; Svatoš, A. *Plant J.* **2018**, *93*, 193−206.
(14) Weissflog, I.; Vogler, N.; Akimov, D.; Dellith, A.; Schachtschabel, D.; Svatos, A.; Boland, W.; Dietzek, B.; Popp, J. *Plant Physiol.* **2010**, *154*, 604−610.
(15) Greene, P. R.; Bain, C. D. *Colloids Surf., B* **2005**, *45*, 174−180.
(16) Kurouski, D. In *Exploring New Findings on Amyloidosis*, Fernández-Escamilla, A. M., Ed.; InTech: Rijeka, Croatia, 2016; pp 73−98.
(17) Koch, K.; Neinhuis, C.; Ensikat, H. J.; Barthlott, W. *J. Exp. Bot.* **2004**, *55*, 711−718.
(18) Kurouski, D. *Vib. Spectrosc.* **2017**, *91*, 3−15.
(19) Verma, P. *Chem. Rev.* **2017**, *117*, 6447−6466.
(20) Deckert-Gaudig, T.; Taguchi, A.; Kawata, S.; Deckert, V. *Chem. Soc. Rev.* **2017**, *46*, 4077−4110.
(21) Wang, X.; Huang, S. C.; Huang, T. X.; Su, H. S.; Zhong, J. H.; Zeng, Z. C.; Li, M. H.; Ren, B. *Chem. Soc. Rev.* **2017**, *46*, 4020−4041.
(22) Jin, M.; Lu, F.; Belkin, M. *Light: Sci. Appl.* **2017**, *6*, No. e17096.
(23) Dazzi, A.; Prater, C. B. *Chem. Rev.* **2017**, *117*, 5146−5173.
(24) Centrone, A. *Annu. Rev. Anal. Chem.* **2015**, *8*, 101−126.
(25) Ramer, G.; Aksyuk, V. A.; Centrone, A. *Anal. Chem.* **2017**, *89*, 13524−13531.
(26) Perez-Guaita, D.; Kochan, K.; Batty, M.; Doerig, C.; Garcia-Bustos, J.; Espinoza, S.; McNaughton, D.; Heraud, P.; Wood, B. R. *Anal. Chem.* **2018**, *90*, 3140−3148.
(27) Strelcov, E.; Dong, Q.; Li, T.; Chae, J.; Shao, Y.; Deng, Y.; Gruverman, A.; Huang, J.; Centrone, A. *Sci. Adv.* **2017**, *3*, No. e1602165.
(28) Dazzi, A.; Prater, C. B.; Hu, Q.; Chase, D. B.; Rabolt, J. F.; Marcott, C. *Appl. Spectrosc.* **2012**, *66*, 1365−1384.
(29) Colthup, N. B.; Daly, L. H.; Wiberley, S. E. *Introduction to Infrared and Raman Spectroscopy*, 3rd ed.; Academic Press: San Diego, CA, USA, 1990.
(30) Heredia-Guerrero, J. A.; Benitez, J. J.; Dominguez, E.; Bayer, I. S.; Cingolani, R.; Athanassiou, A.; Heredia, A. *Front. Plant Sci.* **2014**, *5*, 305.
(31) MFA Museum of Fine Arts Boston, CAMEO Materials Database: http://cameo.mfa.org/wiki/Microcrystalline_wax, 2016.
(32) Avato, P.; Bianchi, G.; Mariani, G. *Phytochemistry* **1984**, *23*, 2843.
(33) Chamel, A.; Maréchal, Y. *C. R. Acad. Sci. Paris* **1992**, *315*, 347−354.
(34) Ensikat, H. J.; Boese, M.; Mader, W.; Barthlott, W.; Koch, K. *Chem. Phys. Lipids* **2006**, *144*, 45−59.
(35) Koch, K.; Ensikat, H. J. *Micron* **2008**, *39*, 759−772.
(36) Carlton, R. A. In *Pharmaceutical Microscopy*; Springer, 2011; pp 7−64.
(37) Schönherr, J.; Baur, P. *Pestic. Sci.* **1994**, *42*, 185−208.
(38) Schönherr, J. *J. Plant Nutr. Soil Sci.* **2001**, *164*, 225−231.
(39) Schönherr, J. *Planta* **2000**, *212*, 112−118.
(40) Schreiber, L. *Ann. Bot.* **2005**, *95*, 1069−1073.
(41) Mendgen, K. In *Plant Cuticles*; Kerstiens, G., Ed.; BIOS: Oxford, 1996; pp 175−188.
(42) Nicholson, R. L.; Kunoh, H.; Shiraishi, T.; Yamada, T. *Physiol. Mol. Plant Pathol.* **1993**, *43*, 307−318.
(43) Kirkwood, R. C. *Pestic. Sci.* **1999**, *55*, 69−77.

DOI: 10.1021/acs.analchem.8b05294
Anal. Chem. XXXX, XXX, XXX−XXX